Journal of Materials Chemistry A

Accepted Manuscript

ROYAL SOCIETY OF CHEMISTRY

www.rsc.org/materialsA

Pine Cone Shells-Based Activated Carbon Used for CO_2 Adsorption

Kaimin Li, [a] *Sicong Tian,* [a] *Jianguo Jiang,* *[a, b, c] *Jiaming Wang,* [a] *Xuejing Chen,* [a] *Feng Yan* [a]

[a] School of Environment, Tsinghua University, Beijing 100084, China

[b] Key Laboratory for Solid Waste Management and Environment Safety, Ministry of Education of China, Beijing 100084, China

[c] Collaborative Innovation Center for Regional Environmental Quality, Tsinghua University, Beijing 100084, China

* Email: jianguoj@tsinghua.edu.cn

Abstract:

For the first time, pine cone shell-based activated carbons were used to adsorb CO_2. After a carbonation process at 500 ^oC, the resulting preliminary activated carbons (Non-PAC) were activated under different conditions. The results indicated a good CO_2 adsorption performance of pine cone shell-based activated carbons. For example, after activation at 650 ^oC and a KOH:Non-PAC ratio of 2, the activated carbon (named as PAC-650/2) achieved a high CO_2 adsorption capacity of 7.63 mmol/g and 2.35 mmol/g at 0 ^oC under 1 and 0.15 bar pressure, respectively. To determine the potential correlation between amounts of CO_2 adsorbed and micropore distribution, linear correlations between cumulative pore volume over different ranges and amounts of CO_2 adsorbed were analyzed. Results showed that pores < 0.70 nm played an important role in the CO_2 adsorption process at 0 ^oC and 0.1 bar, and contrary to previous research, pore volume of pores < 0.80 nm or 0.82 nm had not good linear correlation with amounts of CO_2 adsorption at 0 ^oC and 1 bar, and we inferred that this most likely due to the unique pore structure

of pine cone shell-based activated carbons. The highest Brunauer-Emmett-Teller (BET) surface area of 3931 m^2/g was obtained after activation at 800 ^oC and KOH:Non-PAC ratio of 2, but the highest BET surface area did not result in the highest CO_2 adsorption capacity. This mainly due to the BET surface area having regions unavailable for CO_2 adsorption. X-ray photoelectron spectroscopy (XPS) analysis results for all activated carbons indicating a higher stability of pyrodonic-N than that of pyridininc-N. Furthermore, in order to better learn the interaction between CO_2 and pine cone shell-based activated carbons, we had analyzed the isosteric heat of adsorption (Q_{st}). The Q_{st} was higher than 22 kJ/mol for all activated carbons, and the highest initial isosteric heat of adsorption of 32.9 kJ/mol was obtained by the activated carbon activated at 500 ^oC and a KOH:Non-PAC ratio of 1. The optimal Q_{st} ($Q_{st,opt}$) under a vacuum swing adsorption (VSA) process was 30 kJ/mol.

Introduction

In 2014, the concentration of long-lived greenhouse gases (LLGHGs) in the atmosphere reached the CO_2-equivalent mole fraction of 481 ppm, and the concentration of CO_2 itself accounted for 83% of this Fig. and reached 397.7 ppm, which was an increase of 1.9 ppm compared with that in 2013.[1] It is well-known that an increase of CO_2 in the atmosphere leads to an enhanced greenhouse effect and ocean acidification. In essence, the problems caused by CO_2 emission are due to energy production. Fossil fuel combustion is the main reason for the increase in CO_2 concentrations in the atmosphere. The development of new energy sources with zero CO_2 emission is the only way to reduce CO_2 emissions for long-term. However, over the next decades, fossil fuels (coal, oil, and natural gas) will still remain a large part of our primary energy source, therefore, several CO_2 emission reduction measures need to be adopted to mitigate CO_2 emission

and CO_2 capture and storage (CCS) will be a necessary method.[2, 3]

In recent years, many different solid adsorbents, such as activated carbon,[4] zeolite,[5] metal-organic frameworks (MOFs),[6] organic-inorganic hybrid/composite adsorbents,[7, 8] calcium oxide,[9] and others have been developed to substitute traditional amine aqueous solution technology. Of these adsorbents, activated carbon has attracted much interest due to its low cost, good availability, large surface area, easy-to-design pore structure, and low energy requirements for regeneration.[10]

Many studies have been conducted to determine how to improve the CO_2 adsorption performance of activated carbons, especially at a low CO_2 pressure (0.15 bar),[4, 11] while considering the CO_2 adsorption selectivity to N_2 or CH_4.[12] In our opinion, the methods used to prepare activated carbons can be categorized as either traditional or new. Traditional methods used to prepare activated carbons utilize natural plants, plant parts (especially the annually updated parts), or some other cheap C-rich materials as a precursor, through direct carbonation and subsequent activation. New methods generally use pure C-rich chemicals (e.g., sodium alginate,[11] Resorcinol,[4] 4-hexylresorcinol,[4] p-nitrophenol,[4] pyrrole,[13] titanium carbide,[14] acetonitrile, furfuryl alcohol and ethylene[15]) as precursors to synthesize activated carbons, and other auxiliary chemicals (e.g., nitric acid,[11] phosphoric acid,[11] formaldehyde,[4] and ferric trichloride,[13] zeolite and hydrofluoric acid[15]) are also needed in the synthetic process. Furthermore, a hydrothermal carbonization process had also been utilized by some research to prepare carbonaceous materials.[10, 15, 16]

New methods make it easy to obtain highly effective activated carbon with a large CO_2 adsorption capacity and good adsorption selectivity; however, the complex preparation process

also may lead to a cost and time consumption increase. To the best of our knowledge, no process is currently available for the large-scale preparation of activated carbons among the new methods. Therefore, utilizing traditional methods with a good natural carbon-rich precursor to prepare highly effective activated carbons for CO_2 adsorption is still a preferred approach. In recent years, many natural wooden materials such as bamboo,[17] bean dreg,[18] peanut shells,[19] petroleum coke,[20] and others have been used to prepare activated carbons for CO_2 adsorption.

Pine cone shells occur widely in the nature, and some studies had used pine cone shells or pine cone shells-based activated carbons to remove the anionic dye Congo red,[21] Ni^{2+},[22] Pb^{2+},[23] Cr^{6+},[24] phenol,[24] and Cu^{2+},[25] from aqueous solutions, or had been used as an electrode material.[26] However, there has been no reports of the use of pine cone shells-based activated carbons for CO_2 adsorption.

In this study, pine cone shells were used as precursors to prepare activated carbons. By varying the activation temperature and KOH dosage in the activation process, a series of activated carbons were obtained. Through analyzing the effects of activation temperature and KOH dosage on micropores distribution, specific surface area, and elemental N content and nitrogen groups species, further determine the influence of activation temperature and KOH dosage on CO_2 adsorption and adsorption selectivity to N_2 of pine cone shells-based activated carbons. In order to determine the relationship between micropores and amounts of CO_2 adsorbed, the linear relationship between them will be built, and further ensure the role of micropores with different size in CO_2 adsorption process. Moreover, in order to better learn the CO_2 adsorption behavior of pine cone shells-based activated carbons, the isosteric heat of CO_2 adsorption was analyzed for all activated carbons, and the optimal isosteric heat of adsorption under a certain vacuum swing

adsorption (VSA) condition will be analyzed. And finally, the optimal preparation strategy for pine cone shells-based activated carbons was determined, which enables a good balance among CO_2 adsorption capacity, adsorption selectivity, and preparation costs.

Experiments

Materials

The pine cone shells used as precursors for preparing activated carbons were collected from pine trees on the campus of Tsinghua University (Beijing, China). Potassium hydroxide (99.98% [metal basis]) was purchased form Alfa Aesar (Ward Hill, MA, US). Hydrochloric acid (38%) was purchased form Sinopharm Chemical Reagent Co., Ltd (Beijng, China), and CO_2 (99.999%), N_2 (99.999%), and He (99.999%) were supplied by ZG special gas (Beijing, China).

Preparation of activated carbon

First, clean pine cone shells were placed in a tube oven and heated from room temperature (RT) to 500 ^oC at a heating rate of 5 ^oC/min in an N_2 atmosphere. The pine cone shells was carbonized at 500 ^oC for 2 h (in Fig. S1, a temperature programming test for pine cone shells shows that 500 ^oC is good choice for the carbonation process, and in Fig. S2, the SEM images for pine cone shells before and after carbonation showed obvious difference in surface and pore structure). When the temperature of the tube oven decreased to RT, 1 g of the preliminary activated carbon (Non-PAC) and an appropriate amount of KOH (1, 2, 3, or 4 g) was added. The KOH and Non-PAC were thoroughly ground and mixed in a ratio denoted as χ (χ = 1, 2, 3, or 4). The mixture was placed in a tube oven and heated from RT to a γ ^oC (i.e., 500, 550, 600, 650, 700, 750, or 800 ^oC) at a heating rate of 3 ^oC/min under an N_2 atmosphere 60 mL/min, after which the mixture was held for 1 h at γ ^oC. When the temperature of the tube oven decreased to RT, the mixture was placed into

50 mL deionized water and desirable hydrochloric acid was added. The solution was stirred for 5 min. Finally, suction filtration was applied and the residue was thoroughly washed with deionized water and dried at 105 ^{o}C for 3 h. The resulted activated carbons were named as PAC-γ/χ, where γ refers to the activation temperature and χ refers to the KOH:Non-PAC ratio. In table S1, the elemental C, O, N, and H content were summarized for all activated samples.

Characterization

CO_2 and N_2 adsorption results under a certain temperature and pressure were obtained using an ASAP 2020 analyzer (Micromeritics, USA). Micropore distribution was calculated using the nonlocal density functional theory (NLDFT) method from the CO_2 adsorption at 0 ^{o}C. Surface area was calculated using a Brunauer-Emmett-Teller (BET) model from the N_2 adsorption data at -196 ^{o}C in the relative pressure (P/P_0) ranging from 0.01 to 0.05. When used for the first time, all activated carbons were degassed for 12 h, with the ASAP 2020 analyzer under a high vacuum degree at 300 ^{o}C. X-ray photoelectron spectroscopy (XPS) results were obtained with an ESCALAB 250XL electron spectrometer (Thermo Scientific, USA) using Al-Kα radiation. The binding energy was referenced to the C1s line at 284.4 eV. Elemental N content results were obtained with a Vario EL III elemental analyzer (Elementar, Germany), and each sample was analyzed two times to obtain an average value.

Results and Discussion

The CO_2 and N_2 adsorption results are shown in Figs. 1 and 2, with the CO_2 adsorption isotherms at 0, 25, and 45 ^{o}C, and the N_2 adsorption isotherms at 25 ^{o}C obtained for all activated carbons. As shown in Figs. 1 and 2, both activation temperature and KOH dosage influenced the CO_2 and N_2 adsorption performance of the activated carbons.

Fig. 1 shows that when the activation temperature increased from 500 to 550, 600, and 650 ^{o}C, the CO_2 adsorption isotherms rise in turn at 0, 25, and 45 ^{o}C. However, an inverse trend was apparent when the activation temperature was further increased from 650 to 700, 750, and 800 ^{o}C, although at high pressure range, the amount of CO_2 adsorbed slightly increased for PAC-700/2 compared to PAC-650/2 at 0 ^{o}C. At 25 ^{o}C, N_2 adsorption isotherms rise in turn when the activation temperature increased from 500 to 550, 600, and 650 ^{o}C, but the N_2 adsorption isotherms of activated carbons were almost the same when the activation temperature is 650, 700, 750, and 800 ^{o}C.

Fig. 2 shows that when the KOH:Non-PAC ratio increased from 1 to 2, both CO_2 and N_2 adsorption isotherms rise (a slight decrease in the amount of CO_2 adsorbed occurred in the low pressure range, and this refers to a decrease of very narrow micropores in PAC-500/2 compared to PAC-500/1). However, when the KOH:Non-PAC ratio increased to 3, both CO_2 and N_2 adsorption isotherms decline, and when the value further increased to 4, both the CO_2 and N_2 adsorption isotherms of PAC-500/4 were almost the same as those for PAC-500/3. Therefore, considering the CO_2 adsorption capacity, a higher activation temperature or KOH:Non-PAC ratio is not always beneficial for CO_2 adsorption. For pine cone shells-based activated carbons, the best activation temperature and KOH:Non-PAC ratio were 650 ^{o}C and 2, respectively.

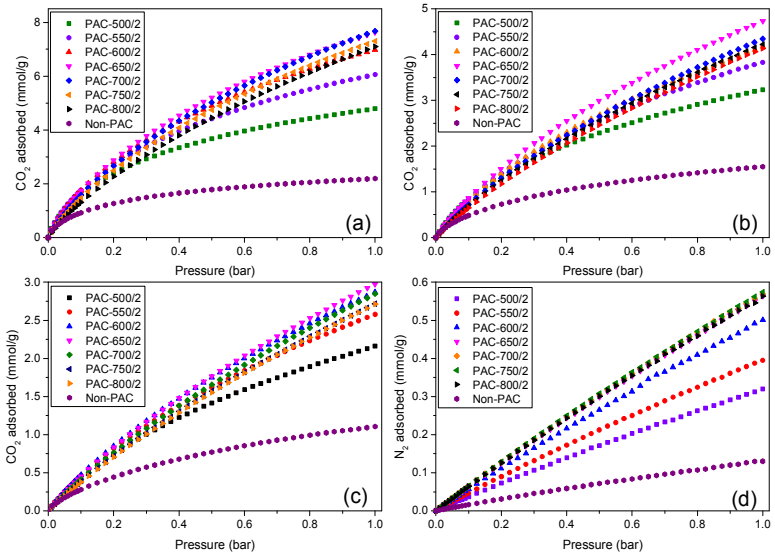

Fig. 1 CO_2 and N_2 adsorption isotherms for activated carbons prepared under different activation temperatures and at a KOH:Non-PAC ratio of 2: (a) for CO_2 adsorption isotherms at 0 ^oC; (b) for CO_2 adsorption isotherms at 25 ^oC; (c) for CO_2 adsorption isotherms at 45 ^oC; (d) for N_2 adsorption isotherms at 25 ^oC.

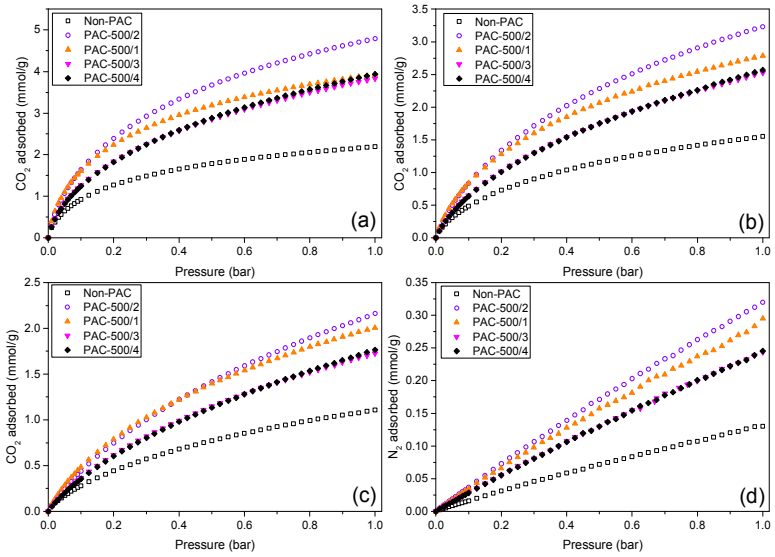

Fig. 2 CO_2 and N_2 adsorption isotherms for activated carbons prepared with different KOH:Non-PAC ratios and under 500 ^oC: (a) for CO_2 adsorption isotherms at 0 ^oC; (b) for CO_2 adsorption isotherms at 25 ^oC; (c) for CO_2 adsorption isotherms at 45 ^oC; (d) for N_2 adsorption

isotherms at 25 ^{o}C.

Considering that flue gas generally contains 15% CO_2, therefore the CO_2 adsorption capacity of activated carbons at 0.15 bar and their adsorption selectivity to N_2 are two important factors for CO_2 capture application of activated carbons. In this work, the adsorption selectivity was calculated with IAST model[12, 27, 28] at 25 ^{o}C and under 1 bar contains 15% CO_2 and 85% N_2 (the experimental CO_2 adsorption isotherms are fitted with single or dual-site Langmuir model, and the experimental N_2 adsorption isotherms are fitted with a single-site Langmuir model), and the adsorption selectivity factor is calculated with formula (1):

$$S_{ads} = \frac{q_1/q_2}{p_1/p_2} \quad (1)$$

where q_i is the amount adsorbed and p_i is the partial pressure of component i.

Fig. 3 shows the CO_2 to N_2 adsorption selectivity for all activated carbons. The CO_2 to N_2 adsorption selectivity is higher than 12, which is high for pure activated carbons.[29] Interestingly, after activation the adsorption selectivity decreases compared with the preliminary activated carbon (Non-PAC), whose adsorption selectivity was 76. With activation temperature increase, the CO_2 to N_2 adsorption selectivity decreased, but with a gradually lower rate and finally reaching a relative constant value. With KOH:Non-PAC increase, the CO_2 to N_2 adsorption selectivity also decreased when the KOH:Non-PAC ratio increased from 1 to 2, but a relative constant value was obtained at KOH:Non-PAC ratios of 2, 3, and 4. These are interesting phenomena and are most likely associated with the activation process, which influences the properties of the activated carbons, and further influence the adsorption selectivity of the activated carbons.

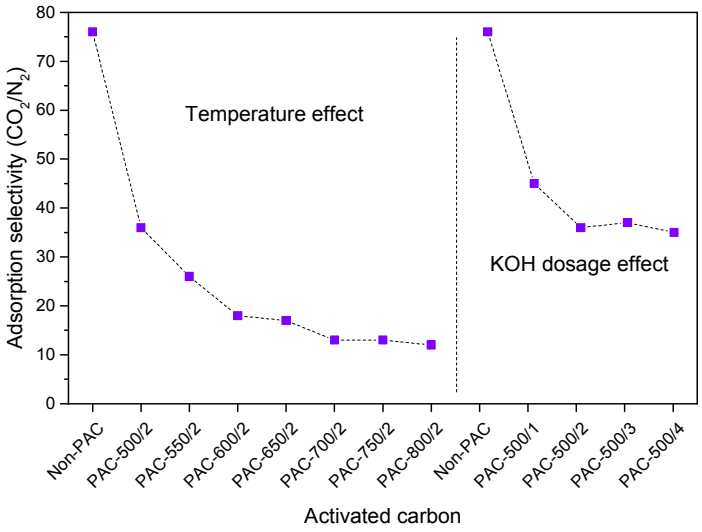

Fig. 3 CO_2 to N_2 adsorption selectivity calculated with the IAST model at 25 ^oC under 1 bar contain 15% CO_2 and 85% N_2 for all activated carbons.

An ideal activated carbon material used for CO_2 capture should obtain a balance in the following aspects: (1) CO_2 capture capacity, especially under 0.15 bar, (2) adsorption selectivity to N_2, and (3) preparation costs. In this study, at 0.15 bar and 25 ^oC, PAC-650/2 had the highest CO_2 adsorption capacity of 1.20 mmol/g, and PAC-500/1 had the highest adsorption selectivity of 45 (Non-PAC was not considered due to its low CO_2 adsorption capacity of 0.62 mmol/g at 25 ^oC and 0.15 bar). Table S2 (ESI) summarized the activated carbons for which the adsorption capacity was more than that of PAC-500/1 at 25 ^oC and 0.15 bar and a comparison was made among them. Although the CO_2 adsorption capacities of the other activated carbons were higher than that of PAC-500/1, the capacity increase was proportionately obviously lower than the decrease in adsorption selectivity. Furthermore, PAC-500/1 was prepared at the lowest temperature and KOH dosage, and is therefore the optimal choice in terms of its practical preparation and application. In Table 1, a comparison in CO_2 adsorption capacity and selectivity to N_2 with others carbon materials, zeolite 13X, and porous polymer materials was summarized for a part of samples in our

study (and the relative data for other samples in our study are listed in table S3 in ESI), indicating a good CO_2 adsorption performance for pine cone shells-based activated carbons.

Table 1 A comparison in CO_2 adsorption performance between the activated carbons used in our study and other carbon materials, zeolite 13X and porous polymer materials.

Sample	BET surface area (m^2/g)	Adsorption capacity (mmol/g)	T (^oC) [a]	P (bar) [b]	S_{ads} [c]	Ref.
E1A1-42	1369	2.45	25	1	NA [d]	30
Bamboo-3-873	1846	7.0/4.5	0/25	1	8.6	17
Bamboo-1-973	930	5.3/4.0	0/25	1	11.1	17
CP-2-600	1700	6.2/3.9/2.1	0/25/50	1	12	13
PC	1220	3.97	25	1	NA	36
AC4-PC	2151	3.64	25	1	NA	36
PC680	1713	7.25/4.41	0/25	1	NA	19
AS-2-600	1260	6.1/4.8/3.6	0/25/50	1	9	10
AS-2-700	1390	6.6/4.3/2.6	0/25/50	1	NA	10
micro-TiC-CDC (700, H_2@600)	1832	(1.51)7.09	0	(0.1)1	NA	14
activated micro-TiC-CDC (500, KOH@600)	3101	(1.18)6.31	0	(0.1)1	NA	14
SK-0.5-700	1060	4.24	25	1	NA	18
NPC-650	1033	5.26/3.10	0/25	1	12.5	40
NPC-750	3199	4.25/2.15	0/25	1	NA	40
SA-2N-P	1740	8.99/4.57/2.98	0/25/45	1	29	11
SA-2N-P	1740	1.51	25	0.15	29	11
SC800	1375	~3.1 [e]	25	1	NA	16
AC-CPD-45%	1292	6.95	0	1	NA	29
MC-200D8H	748	2.73	25	1	NA	38
MC-250D8H	736	2.69/1.01	25/75	1	21.6	38
MC-250D8H	736	0.91	25	0.15	21.6	38
NMC-250D8H	385	2.43/1.66	25/75	1	240.7	38
NMC-250D8H	385	1.16	25	0.15	240.7	38
ACGR2700	1512	(1.5)4.9	25	(0.15)1	NA	32
ACGR4700	3144	(0.9)4.1	25	(0.15)1	NA	32
ACCA2700	1353	(1.5)5.0	25	(0.15)1	NA	32
ACCA4800	3537	(0.6)2.8	25	(0.15)1	NA	32
K4-700	1745	3.45	25	1	8	20
K6-800	3047	2.64	25	1	8.9	20
K5-800	2856	2.73	25	1	10	20

sOMC	NA	3.0/2.0	5/25	1	11.3	12
Zeolite 13X	534	3.30	25	1	29	20
CS-650-1.5	1196	(1.57)4.37	25	(0.15)1	23.1	31
P1	10.7	1.9	0	1	10139	47
PPN-81	NA	1.9	22	1	4716	48
ACM-5	2501	11.51	0	1	NA	49
PAC-500/1	1246	3.93/2.79/2.01	0/25/45	1	45	This work
PAC-500/1	1246	1.97/1.07/0.65	0/25/45	0.15	45	This work
PAC-650/2	3135	7.63/4.73/2.98	0/25/45	1	17	This work
PAC-650/2	3135	2.35/1.20/0.65	0/25/45	0.15	17	This work
PAC-800/2	3931	7.10/4.13/2.71	0/25/45	1	12	This work
PAC-800/2	3931	1.81/0.92/0.55	0/25/45	0.15	12	This work

[a] Adsorption temperature: a diagonal is used to distinguish different adsorption temperatures that correspond to the CO_2 adsorption capacity in the third column in the same row. [b] Adsorption pressure: parentheses are used to distinguish different adsorption pressures that correspond to the CO_2 adsorption capacity in the third column in the same row. [c] CO_2 to N_2 adsorption selectivity was calculated at 25 ^oC. [d] NA means unavailable. [e] The value of CO_2 adsorption capacity is estimated from the figure depicting CO_2 adsorption isotherms, because the authors did not provide an accurate value.

Fig. 4 shows that the pore size distribution of the activated carbons, as calculated by the NLDFT method utilizing the CO_2 adsorption results at 0 ^oC. Figs. S3 and S4 show the N_2 adsorption-desorption isotherms and pore size distribution calculated from the N_2 adsorption results at -196 ^oC using the NLDFT method. The N_2 adsorption-desorption results indicate that all activated carbons consist mainly of micropores; the TEM images (Fig. S5) confirm this for all materials. The pore size distribution (< 1 nm) derived from the CO_2 adsorption at 0 ^oC is different from that derived from the N_2 adsorption results at 0 ^oC (Fig. S4). However, much research confirmed that CO_2 adsorption at 0 ^oC could give a more concise pore size distribution (< 1 nm) than that derived from N_2 adsorption at -196 ^oC. Therefore, the pore size distribution (< 1 nm)

derived from the CO_2 adsorption at 0 ^oC was adopted to analyze the relationship between pore structure and CO_2 adsorption performance. Interestingly, two distinct regions are observed in Fig. 4: region I, ranging from 0.40 nm to 0.70nm; and region II, ranging from 0.70 nm to 1.08 nm. To better understand the relationship between pore size distribution and the amounts of CO_2 adsorbed, we determined the linear correlations between the cumulative pore volumes in different pore size ranges and the amounts of CO_2 adsorbed at 0 ^oC under 1 bar or 0.1 bar. The results are shown in Figs. 5 and 6, respectively.

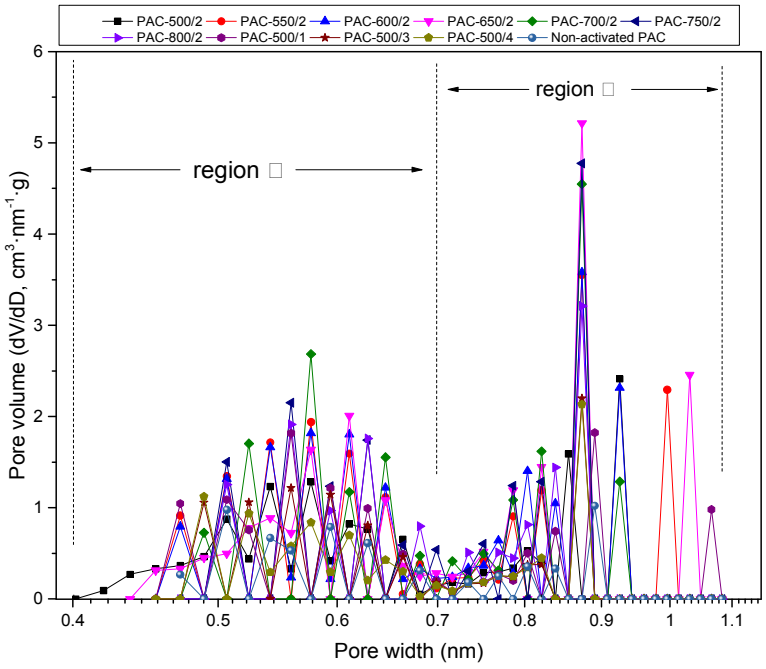

Fig. 4 Micropore distribution of activated carbons calculated using CO_2 adsorption data at 0 ^oC with the NLDFT method.

Previous studies have shown that narrow micropores (<1 nm) are very important in the CO_2 adsorption process of activated carbons under low pressure (1 bar).[10, 30] Further, Presser *et al.*[14] reported that the volume of micropores with a size < 0.80 nm had a very good linear correlation with the amounts of CO_2 adsorbed at 0 ^oC under 1 bar. Wei *et al.*[17] reported a similar results,

suggesting that the volume of micropores with pore sizes < 0.82 nm had a good linear correlation with the amounts of CO_2 adsorbed at 0 ^oC and 1 bar, and further pointed out that a micropore measuring 0.55 nm contributes the most in the adsorption process. Furthermore, Grundy *et al.*[29] reported that pores < 0.6 nm play an important role in the CO_2 adsorption process at 0 ^oC under 1 bar. Chen *et al.*[31] also reported on the role of pores < 0.82 nm and 0.63 nm in the CO_2 adsorption process under 1 bar at 0 ^oC and 25 ^oC, respectively.

As shown in Fig. 5, the linear correlation coefficient (R^2) for the relationship between the pore volume of pore sizes <0.82 nm with the amounts of CO_2 adsorbed at 0 ^oC under 1 bar was only 0.6004 (i.e., far below the value reported by Wei *et al.* [17]). The R^2 for the relationship between the pore volume of pore sizes <0.80 nm with the CO_2 adsorption capacity at 0 ^oC and 1 bar was 0.5240, which was also far lower than the value reported by Presser *et al.* [14] We also determined the correlation between the pore volume of pore sizes <0.70 and 1.0 nm with the CO_2 adsorption capacity at 0 ^oC and 1 bar, and the R^2 values were only 0.3658 and 0.7035, respectively. These results suggest some difference with previous reports.

In Fig. 6, the linear correlation between the cumulative volume and the CO_2 adsorption capacity at 0 ^oC and 0.1 bar had a much better linear correlation. The R^2 values for the relationship between the volume of pores with a size of <0.60, 0.70, 0.72, 0.80, 0.82, and 1.0 nm and the CO_2 adsorption capacity at 0 ^oC and 0.1 bar were 0.7877, 0.9827, 0.9787, 0.9310, 0.9078, and 0.8211, respectively. These data suggest that the pores in region I (0.40-0.70 nm) play an important role in the CO_2 adsorption process at 0 ^oC and 0.1 bar. In the report by Presser *et al.* [14] , they revealed that the pore volume of pores < 0.80 nm had a much better linear correlation with the amounts of CO_2 adsorbed at 0 ^oC under 1 bar (R^2 = 0.9958) than that with the amount of CO_2 adsorbed at 0 ^oC

under 0.1 bar (R^2 = 0.6514). This showed difference with our results. In our research, the pore volume of pores < 0.80 nm had a much better linear correlation with the amounts of CO_2 adsorbed at 0 ^oC under 0.1 bar (R^2 = 0.9310) than that with the amounts of CO_2 adsorbed at 0 ^oC under 1bar (R^2 = 0.5240). In fact, our study showed that the cumulative pore volume of pores < 0.70 nm had the best linear correlation with the amounts of CO_2 adsorbed at 0 ^oC under 0.1 bar (R^2 = 0.9827) and is far better correlated than that with the amounts of CO_2 adsorbed at 0 ^oC under 1bar (R^2 = 0.3658). According to Presser *et al.* [14] , the cumulative pore volume of pores < 0.5 nm exhibited a much better linear correlation with the amounts of CO_2 adsorbed at 0 ^oC and 0.1 bar (R^2 = 0.9468) than that at 0 ^oC and 1 bar (R^2 = 0.6111).

Therefore, our study showed different results compared with previous studies. To account for this phenomenon, we have put forward our interpretation, but further research must be necessary. Unlikely the results reported by Presser *et al.* [14] and Wei *et al.* [17], the pore size distribution of the activated carbons in our study exhibited obvious discontinuity (here, we defined the discontinuity as a point which the pore volume was zero at a certain pore diameter) and multiple peaks properties (Fig. S6 shows more clear information on pore size distribution for each activated carbon in our study). However, according to both Presser *et al.* [14] and Wei *et al.* [17] , pore size distribution shows good continuityand only three or four peaks appeared, and this just like the pore size distributions reported by Grundy *et al.* [29] and Chen *et al.* [31]. It appears that the pores of activated carbons in our study likely consist of those with limited species of pore size, which was different with other researches and this may result in a different CO_2 adsorption process in the pores. Therefore, these inconsistent results may largely be derived from the different pore structures. Furthermore, the nitrogen groups contained in our activated carbons (Fig. 8) may also

contribute to the inconsistent results between our study and previous research.[31] In the study by Presser *et al.* [14], titanium carbide was used as the precursor to synthesize activated carbon with no elemental N introduced, and therefore no elemental N was present in the activated carbon prepared. Wei *et al.* [17] did not report the elemental N content of the bamboo-based activated carbon used in their research.

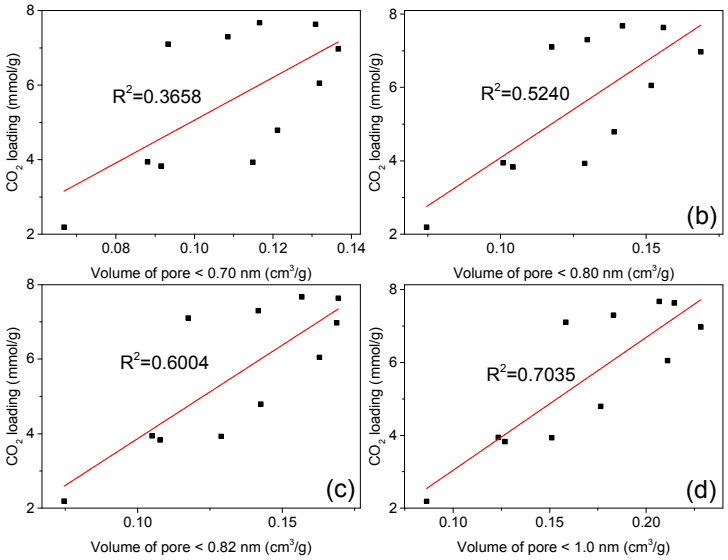

Fig. 5 Linear correlation between the amount of CO_2 adsorbed (0 ^oC, 1 bar) and cumulative pore volume derived from the NLDFT method, with CO_2 adsorption data for different pore sizes: (a) <0.72 nm; (b) <0.80 nm; (c) <0.82 nm; (d) <1.0 nm.

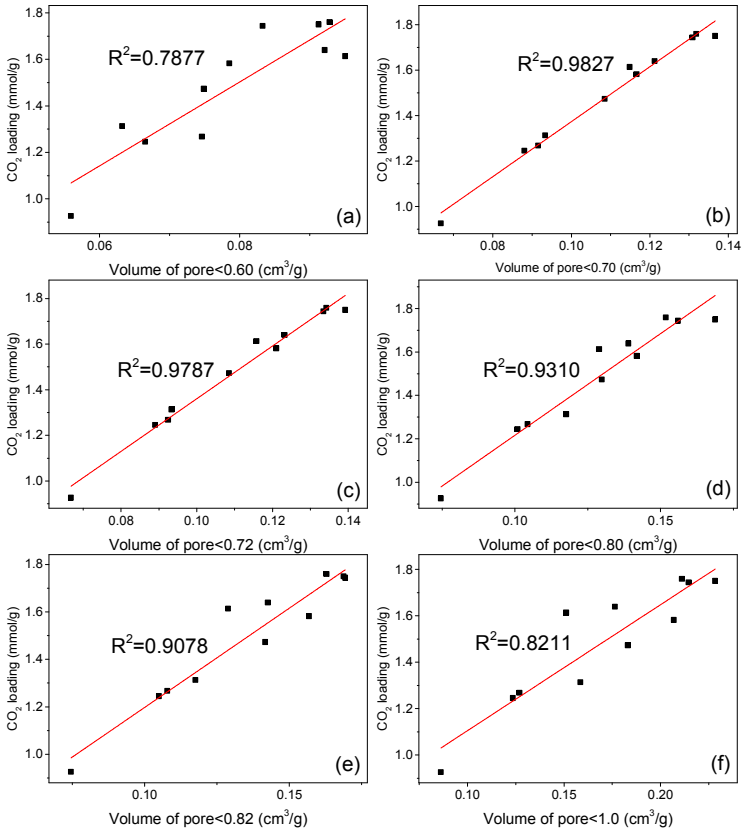

Fig. 6 Linear correlation between the amount of CO_2 adsorbed (0 ^oC, 1 bar) and the cumulative pore volume derived from the NLDFT method, with N_2 adsorption data for different pore sizes: (a) <0.73 nm; (b) <0.80 nm; (c) <0.84 nm; (d) <1.0 nm; (e) <1.5 nm; (f) <2.0 nm.

Fig. 7 shows that the BET surface area of activated carbons increased with activation temperature and the KOH:Non-PAC ratio, except for a slight decrease at an KOH:Non-PAC = 3 (detailed BET surface area data is in Table S4 in ESI). In table 1, a high BET surface area property for pine cone shell-base activated carbons can be confirmed through comparing with other carbon materials. Generally, a large surface area is necessary in the physical adsorption processes, but larger surface area does not always mean larger CO_2 adsorption capacity. In our study, a change in the surface area of the activated carbons was not consistent with changes in CO_2 adsorption capacity. For example, the PAC-800/2 obtains the highest surface area of 3931 m^2/g, but its CO_2

adsorption capacity at 0 °C, 25 °C, and 45 °C under 1 bar is lower than that of PAC-650/2 with a surface area of 3135 m^2/g. A similar result was also reported by Xing *et al.*[18] To explain this phenomenon, we hypothesized that the BET surface area could be divided into an area available for CO_2 adsorption and an area unavailable for CO_2 adsorption under a relative low pressure (such as ≤1 bar). Therefore, an increase in the overall surface area is not always beneficial for CO_2 adsorption, because an increase in the area unavailable for CO_2 adsorption can not result in an increase in CO_2 adsorption capacity under relative low pressure, but the area will be useful for CO_2 adsorption under high pressure (such as 20 bar, 25 bar).[30, 32] The varies in BET surface area of activated carbons was largely associated with the activation process for activated carbons preparation.

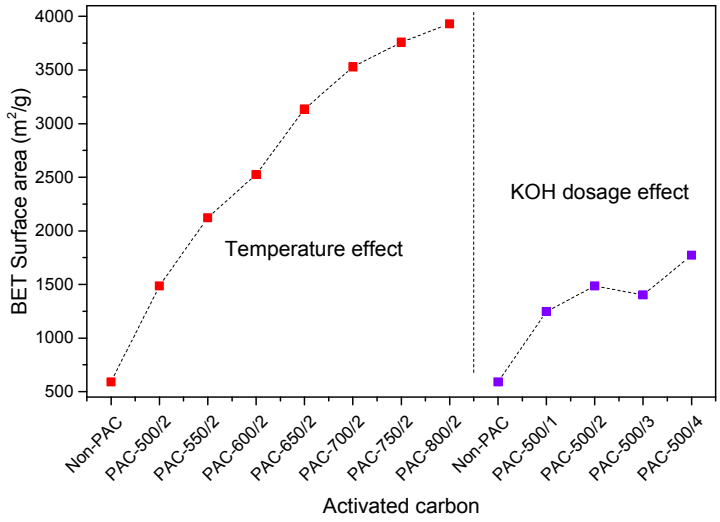

Fig. 7 BET surface area of activated carbons.

In the preparation of activated carbon, an activation process is used to remove the most reactive carbon atoms from the carbon structure, which improves the specific surface area and porosity of the activated carbon.[33] In the activation process, two discrete stages can be identified. The first stage generally is a physical grind and mixing process, in which the diffusivity of solid

KOH is very weak, because it does not easily diffuse into the deep and very narrow micropores. Therefore, some research instead of a grinding process, utilizing a solid-liquid (KOH aqueous solution) diffusion process to strengthen the KOH diffusion.[19, 34] The second stage is a temperature programming and isothermal process, in which the following reactions occur:[33, 35]

$$6KOH + 2C \leftrightarrow 2K + 3H_2 + 2K_2CO_3 \quad (1)$$

$$K_2CO_3 \leftrightarrow K_2O + CO_2 \quad (2)$$

$$K_2CO_3 + C \leftrightarrow K_2O + 2CO \quad (3)$$

$$K_2O + C \leftrightarrow 2K + CO \quad (4)$$

$$2K + CO_2 \leftrightarrow K_2O + CO \quad (5)$$

In the reaction process, carbon is oxidized to K_2CO_3, CO, and CO_2. In this work, the Raman spectrum (Fig. S7) were used to analyze the carbon atoms in activated carbons. Before and after activation, two obvious peaks at 1338-1365 cm^{-1} (D band) and 1587-1592 cm^{-1} (G band) appears in the Raman spectrum of activated carbons. D band is attributed to the structure defects, amorphous carbons or edges that can break the symmetry,[11, 37, 38] and G band is attributed to the in-plane stretching of sp^2-bond carbon atoms in the graphite layer.[11, 37, 38] The integral intensity ration of the two peaks (I_D/I_G) is higher than 1.01 for all activated carbons, referring to abundant defective structure and poor graphitization in pine cone shell-based activated carbons.[36, 37, 38] Moreover, the I_D/I_G exhibited some increase after activation, on one hand confirming the reaction between carbon atoms and KOH in the activation process, and on the other hand indicating the increase of disorder carbons at the cost of sp^2-bond carbon atoms without dangling bond. [36] Furthermore，the SEM images (Fig. S2) for Non-PAC and PAC-650/2 show obvious difference between the surface of them, and seems also reflecting the change of carbon structure after

activation.

In activation process, when carbon was oxidized, the KOH is reduced to H_2 and K metals.[33, 35, 39] The K metals plays a secondary but important role in the activation process, with some of it vaporizing under the high temperature, while some K intercalates into the carbon structure.[33, 35, 39] And this may lead to an increase in the graphene interlayer distance, which will result in a better distribution of the remaining KOH into the carbon structure,[39] and therefore increase the porosity of the activated carbon.

According to Linares-Solano *et al.* ,[39] the chemical reactions commence at approximately 280 ^{o}C, before KOH melts (the melting point of KOH is 360–380 ^{o}C), but reaction (1) is the main reaction during the activation process of activated carbons. Reaction (1) begins to fast occur at approximately 400 ^{o}C, which is higher than the melting point of KOH. Therefore, a solid-solid/solid-liquid reaction happens in the activation process,[40] but the chemical reactions mainly proceed after the KOH melts (with the solid-liquid reaction dominating). Because a heating rate of 3 ^{o}C/min is generally used in the activation process, we believe that before reaction (1) commences, liquid KOH has been adequately diffused. In the activation process, small micropores form initially and then some become larger, even reaching mesopore size.[39] In our study, as the activation temperature or KOH dosage increases, the BET surface area and total pore volume (Table S4 in SEI) of activated carbons increase, but is not consistent with the change of CO_2 adsorption capacity of the activated carbons. This is most likely due to a larger micropore or smaller mesopore, which are not available for CO_2 adsroption. These are generally caused by excessive activation, which leads to the destruction of some tyoes of micropore structures by excessive KOH[36] or ultrahigh activation temperatures.[41, 42]

The increase in activation temperature and KOH dosage generates more pores and surface area that are unavailable for CO_2 and N_2 adsorption, and hence the amount of CO_2 and N_2 adsorbed, and the adsorption selectivity of CO_2 to N_2 displays little change above a certain activation temperature and KOH dosage. Therefore, the variations in surface area and porosity due to the activation effect are not always beneficial for CO_2 adsorption.

The presence of N-containing groups in the activated carbon matrix is an important factor that influences the CO_2 adsorption performance of activated carbon.[13] Fig. 8(l) showed that after activation the elemental N content of activated carbons decreased compared to the preliminary activated carbon (Non-PAC). To analyze the properties of elemental N in the activated carbons, XPS was used. In Fig. 8 (a)-(k), the N 1s peaks for all activated carbons except PAC-800/2 can be divided into two peaks, which represent pyridinic nitrogen at binding energies of 397.3-398.7 eV[4, 11, 13] and pyrrolic[4, 11, 13, 40] or pyridonic[13, 40] nitrogen at binding energies of 400.0-400.8 eV, respectively. However, under a high temperature and oxidizing environment the peak at binding energies of 400.0-400.8 eV is most likely attributed to pyridonic nitrogen.[13]

For PAC-800/2, only one peak with a center at a binding energy of 400.2 eV (representing pyrodonic nitrogen) was apparent, and the peak of pyridinic nitrogen was absent. In fact, for PAC-700/2 and PAC-750/2, the pyridininc nitrogen peak had been not clear. This may refers to a higher thermostability of pyrodonic nitrogen groups than that of pyridinic nitrogen groups.

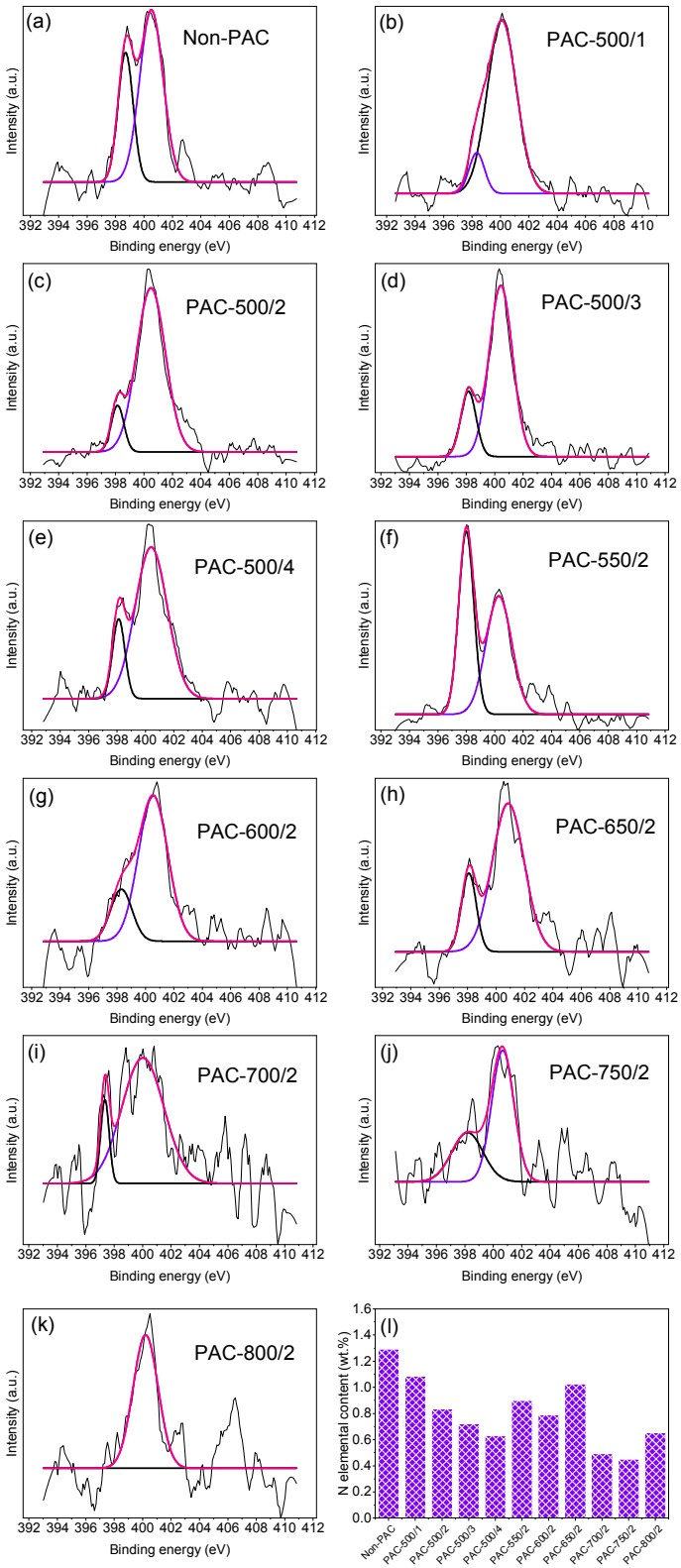

Fig. 8 N 1s XPS spectrum of the activated carbons: (a) for Non-PAC; (b) for PAC-500/1; (c) for

PAC-500/2; (d) for PAC-500/3; (e) for PAC-500/4; (f) for PAC-550/2; (g) for PAC-600/2; (h) for PAC-650/2; (i) for PAC-700/2; (j) for PAC-750/2; (k) for PAC-800/2, and (l) for the elemental N content for all activated carbons.

The regeneration energy consumption of a CO_2 adsorption material is an important factor that influences its practical application. For adsorption materials, the required regeneration energy approximately equals the CO_2 adsorption heat and the sensible heat of the constituent materials,[43] with a particular dependence on the CO_2 adsorption heat.[28] The isosteric heat of adsorption (Q_{st}) is commonly used to estimate the required regeneration heat for an activated carbon used to capture CO_2.[11, 12, 40] The Q_{st} is determined as follows:

$$Q_{st} = RT^2 \left(\frac{\partial lnp}{\partial T}\right)_q \quad (2)$$

For the calculation of Q_{st}, a single-site or dual-site Langmuir model[11, 28, 36, 44] are used to fit with CO_2 adsorption isotherms for all activated carbons at 0, 25, and 45 ^oC (details of the fitting results are provided in the ESI).

Fig. 9 shows that the Q_{st} for all activated carbons was ≥22 kJ/mol, and in Table S7 (ESI) PAC-500/1 has the highest initial isosteric heat of CO_2 adsorption of 32.9 kJ/mol (a value was very similar to the results reported by Xia *et al.*[15] and Cai *et al.*[36]), and referring to the highest initial adsorption potential. And PAC-800/2 has the lowest initial adsorption potential with the lowest initial isosteric heat of CO_2 adsorption of 24.3 kJ/mol. In CO_2 adsorption process in activated carbons, CO_2 is first adsorbed by the most active adsorption site and generating the highest adsorption heat; similarly, a non-active adsorption site will produce lower adsorption heat. In the CO_2 adsorption process, the relative magnitude of the CO_2-activated carbons and CO_2-CO_2 interactions also influence the isosteric heat of CO_2 adsorption;[11, 45] therefore, a change in the

relative magnitude of the CO_2-activated carbons and CO_2-CO_2 interactions as the CO_2 loading increases would affect Q_{st} during the CO_2 adsorption process, and thus result in the first rise-then decline or rise-decline-rise-decline type cures of Q_{st}, as shown in Fig. 9.

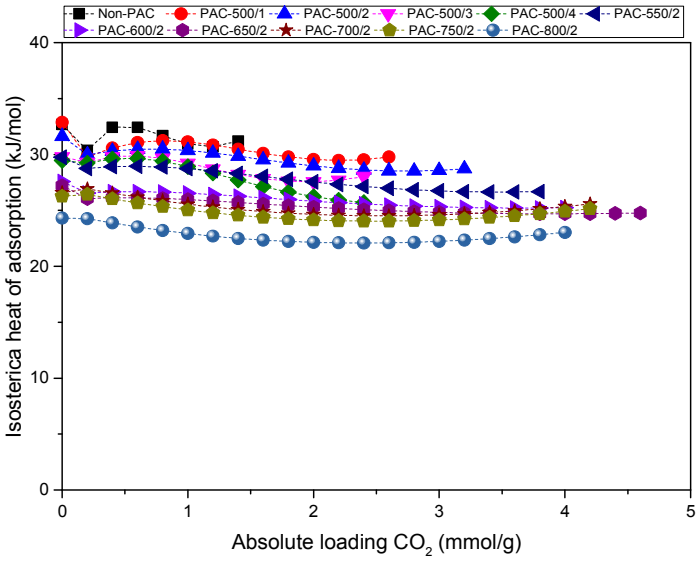

Fig. 9 Isosteric heat of adsorption calculated by the dual-site Langmuir isotherm fits at 0, 25, and 45 ^{o}C.

Fig. 10 shows 20 cycles of CO_2 adsorption for PAC-500/1. For each cycle, the saturation CO_2 adsorption capacity was similar, which indicates a thorough desorption during every regeneration cycle under the vacuum swing adsorption (VSA) process: adsorption at 25 ^{o}C and under 1 bar, and desorption at 25 ^{o}C under 0.01 bar. To better understand the VSA process, the optimal isosteric heat of adsorption was calculated using the following formula:[45, 46]

$$-Q_{st,opt} = \Delta H^{o}_{opt} = T\Delta S^{o} + \frac{RT}{2}\ln\left(\frac{P_1 P_2}{P_o^{\,2}}\right) \qquad (3)$$

where R is the gas constant, T is temperature, P_1 and P_2 are the high and low pressure during the VSA process, respectively, and ΔS^{o} is the entropy change relative to the standard pressure (1 bar). Here, we taking ΔS^{o} = -80 J mol^{-1} K^{-1},[45] and when T = 25 ^{o}C, P_1 = 1 bar, and P_2 = 0.01 bar, and the $Q_{st,opt}$ = 30 kJ/mol. Therefore, for all activated carbons in this work, the Q_{st} was near to the $Q_{st,opt}$,

especially for PAC-500/1, PAC-500/2, PAC-500/3, and PAC-550/2

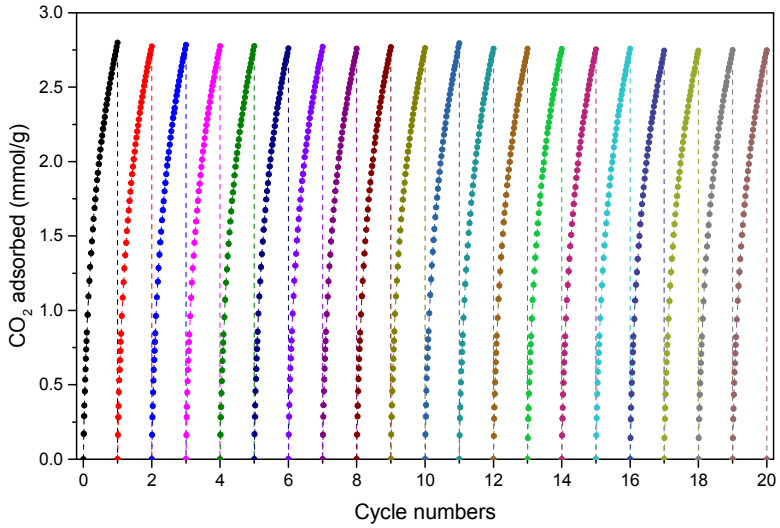

Fig. 10 Twenty cycles of CO_2 adsorption for PAC-500/1 with adsorption at 25 ^{o}C and desorption at 25 ^{o}C under 0.01 bar pressure.

Conclusions

Utilizing pine cone shells as precursors can achieve activated carbon with a high BET surface area of 3931 m^2/g under activation conditions of 800^{o}C and under a KOH:Non-PAC ratio of 2 (PAC-800/2). The highest BET surface area did not result in the highest CO_2 adsorption capacity. PAC-650/2 had a significantly lower BET surface area (3135 m^2/g) than PAC-800/2, but possessed a larger CO_2 adsorption capacity. This is most likely because there is a significant amount of area unavailable for CO_2 adsorption contained in the activated carbons. Considering the CO_2 adsorption capacity, adsorption selectivity, and preparation costs, the pine cone shells-based activated carbon named PAC-500/1 was the best choice than others in our study.

For pine cone shells-based activated carbons, two types of nitrogen groups exist in the activated carbon matrix, however, the XPS spectrum analysis results suggest a higher stability of pyrodonic-N than that of pyridininc-N.

In our study, we analyzed the relationship between micropore volume over different ranges and amounts of CO_2 adsorbed. Our results showed that pores < 0.7 nm play an important role in the CO_2 adsorption process at 0 ^oC under 0.1 bar. Contrary to previous researches, in our study, pores < 0.80 nm or 0.82 nm do not appear to dominate the CO_2 adsorption process at 0 ^oC under 1 bar. We infer that the most likely reason for the different results is that the different property of pore size distribution of pine cone shell-based activated carbons.

Furthermore, to better understand the CO_2 adsorption behavior of pine cone shell-based activated carbons, we analyzed the isosteric heat of CO_2 adsorption (Q_{st}). The results showed that the Q_{st} for all activated carbons was higher than 22 kJ/mol, and PAC-500/1 possessed the highest initial Q_{st}, with 32.9 kJ/mol, referring to the highest initial CO_2 adsorption potential. Moreover, the optimal Q_{st} under a VSA process (adsorption at 25 ^oC under 1 bar and desorption at 25 ^oC under 0.01 bar) of PAC-500/1 was 30 kJ/mol, which is very close to the Q_{st} of PAC-500/1.

Acknowledgement

The authors gratefully acknowledge the support from National Natural Science Foundation of China (Grant No.21576156) and Tsinghua University Initiative Scientific Research Program (Grant No. 2014z22075) in the process of this work carried out.

Electronic supplementary information

We have summarized detailed data of CO_2 and N_2 adsorption under certain adsorption temperatures and pressures, BET surface area, total pore volume, and initial isosteric heat of CO_2 adsorption in the electronic supplementary information. The SEM images for some samples, the Raman spectrum, and relative analytical results were also attached in the electronic supplementary information. Furthermore, we also list the fitting process for CO_2 and N_2 adsorption isotherms

with single-site or dual-site Langmuir model (and the fitting results), as well as the calculation process for initial isosteric heat of adsorption in the electronic supplementary information.

References

1 World Meteorological Organization, Greenhouse Gas Bulletin-The State of Greenhouse Gases in the Atmosphere, 2015, 11, No. 11.

2 U.S. Energy Information Administration, Annual Energy Outlook, 2015, 2015, 4.

3 International Energy Agency, Energy Technology Perspective 2015, 2015.

4 N. López-Salas, M. C. Gutiérrez, C. O. Ania, J. L. G. Fierro, M. L. Ferrer and F. del Monte, *J. Mater. Chem. A*, 2014, **2**, 17387.

5 T. D. Pham, M. R. Hudson, C. M. Brown and R. F. Lobo, *ChemSusChem*, 2014, **7**, 3031.

6 G. Férey, C. Serre, T. Devic, G. Maurin, H. Jobic, P. L. Llewellyn, G. De Weireld, A. Vimont, M. Daturif and J.-S. Chang, *Chem. Soc. Rev.*, 2011, **40**, 550.

7 K.-M. Li, J.-G. Jiang, S.-C. Tian, X.-J. Chen and F. Yan, *J. Phys. Chem. C*, 2014, **118**, 2454.

8 K. Li, J. Jiang, S. Tian, F. Yan and X. Chen, *J. Mater. Chem. A*, 2015, **3**, 2166.

9 A. Sanna, M. Uibu, G. Caramanna, R. Kuusik, M. M. Maroto-Valer, *Chem. Soc. Rev.*, 2014, **43**, 8049.

10 M. Sevilla and A. B. Fuertes, *Energy Environ. Sci.*, 2011, **4**, 1765.

11 X. Ma, Y. Li, M. Cao and C. Hu, *J. Mater. Chem. A*, 2014, **2**, 4819.

12 B. Yuan, X. Wu, Y. Chen, J. Huang, H. Luo and S. Wei, *Environ. Sci. Technol.*, 2013, **47**, 5474.

13 M. Sevilla, P. Valle-Vigón and A. B. Fuertes, *Adv. Funct. Mater.*, 2011, **21**, 2781.

14 V. Presser, J. McDonough, S.-H. Yeon and Y. Gogotsi, *Energy Environ. Sci.*, 2011, **4**, 3059.

15 Y. Xia, R. Mokaya, G. S. Walker and Y. Zhu, *Adv. Energy Mater.*, 2011, **1**, 678.

16 A. S. Mestre, C. Freire, J. Pires, A. P. Carvalho and M. L. Pinto, *J. Mater. Chem. A*, 2014, **2**, 15337.

17 H. Wei, S. Deng, B. Hu, Z. Chen, B. Wang, J. Huang and G. Yu, *ChemSusChem*, 2012, **5**, 2354.

18 W. Xing, C. Liu, Z. Zhou L. Zhang, J. Zhou, S. Zhuo, Z. Yan, H. Gao, G. Wang and S. Z. Qiao, *Energy Environ. Sci.*, 2012, **5**, 7323.

19 D. Li, Y. Tian; L. Li, J. Li, H. Zhang, *J. Porous Mat.*, 2015, **22**, 1581.

20 X. Hu. M. Radosz, K. A. Cychosz and M. Thommes, *Environ. Sci. Technol.*, 2011, **45**, 7068.

21 S. Dawoodand T. K. Sen, *Water Res.*, 2012, **46**, 1933.

22 A. I. Almendros, M. A. Martín-Lara, A. Ronda, A. Pérez, G. Blázquez and M. Calero, *Bioresour. Technol.*, 2015, **196**, 406.

23 M. Momčilović, M. Purenović, A. Bojić, A. Zarubicaand M. Ranđelović, *Desalination*, 2011, **276**, 53.

24 G. Duman, Y. Onal, C. Okutucu, S. Onenc and J. Yanik, *Energy Fuels*, 2009, **23**, 2197.

25 A. E. Ofomaja and E. B. Naidoo, *Chem. Eng. J.*, 2011, **175**, 260.

26 K. Karthikeyan, S. Amaresh, S. N. Lee; X. Sun, V. Aravindan; Y.-G. Lee and Y. S. Lee, *ChemSusChem*, 2014, **7**, 1435.

27 A. L. Myers and J. M. Prausnitz, *AICHE J.*, 1965, **11**, 121.

28 J. A. Mason, K. Sumida, Z. R. Herm, R. Krishna and J. R. Long, *Energy Environ. Sci.*, 2011, **4**, 3030.

29 M. Grundy and Z. Ye, *J. Mater. Chem. A*, 2014, **2**, 20316.

30 C. F. Martín, M. G. Plaza, S. García, J. J. Pis, F. Rubiera and C. Pevida, *Fuel*, 2011, **90**, 2064.

31 T. Chen, S. Deng, B. Wang, J. Huang, Y. Wang and G. Yu, *RSC Adv.*, 2015, **5**, 48323.

32 H. M. Coromina, D. A. Walsh and R. Mokaya, *J. Mater. Chem. A*, DOI: 10.1039/c5ta09202g.

33 V. Jiménez, P. Sánchez, A. de Lucas, J. L. Valverde and A. Romero, *J. Colloid Interface Sci.*, 2009, **336**, 226.

34 L.-Y. Meng and S.-J. Park, *J. Colloid Interface Sci.*, 2010, **352**, 498.

35 V. Jiménez, A. Ramírez-Lucas, J. A. Díaz, P. Sánchez and A. Romero, *Environ. Sci. Technol.*, 2012, **46**, 7407.

36 J. Cai, J. Qi, C. Yang and X. Zhao, *ACS Appl. Mater. Interfaces*, 2014, **6**, 3703.

37 J. Shan, Y. Liu, Y. Su, P. Liu, X. Zhuang, D. Wu, F. Zhang and X. Feng, *J. Mater. Chem. A*, DOI: 10.1039/c5ta08109b.

38 Z. Zhang, B. Wang, C. Zhu, P. Gao, Z. Tang, N. Sun, W. Wei, and Y. Sun, *J. Mater. Chem. A*, 2015, **3**, 23990.

39 J. A. Maciá-Agulló, B. C. Moore, D. Cazorla-Amorós, A. Linares-Solano, *Microporous Mesoporous Mat.*, 2007, **101**, 397.

40 J. Wang, I. Senkovska, M. Oschatz, M. R. Lohe, L. Borchardt, A. Heerwig, Q. Liu and S. Kaskel, *J. Mater. Chem. A*, 2013, **1**, 10951.

41 F. Banisheykholeslami, A. A. Ghoreyshi, M. Mohammadi and K. Pirzadeh, *Clean-Soil Air Water*, 2015, **7**, 1084.

42 J. S. Tan and F. N. Ani, *Sep. Purif. Technol.*, 2004, **1**, 47.

43 K. Li, J. Jiang, F. Yan S. Tian and X. Chen, *Appl. Energy*, 2014, **136**, 750.

44 W. Lu, J. P. Sculley, D. Yuan, R. Krishna, Z. Wei and H.-C. Zhou, *Angew. Chem. Int. Ed.*, 2012, **51**, 7480.

45 J. M. Simmons, H. Wu, W. Zhou and T. Yildirim, *Energy Environ. Sci.*, 2011, **4**, 2177.

46 S. K. Bhatia, *Langmuir*, 2006, **4**, 1688.

47 Y.-Q. Shi, J. Zhu, X.-Q. Liu, J.-C. Geng, L.-B. Sun, *ACS Appl. Mater. Interfaces*, 2014, **6**, 20340.

48 L.-B. Sun, A.-G. Li, X.-D. Liu, X.-Q. Liu, D. Feng, W. Lu, D. Yuan, H.-C. Zhou, *J. Mater. Chem. A*, 2015, **3**, 3252.

49 N. Nandi, K. Okada, A. Dutta, A. Bhaumik, J. Maruyama, D. Derks, H. Uyama, *Chem. Commun*., 2012, **48**, 10283.

The English in this document has been checked by at least two professional editors, both native speakers of English. For a certificate, please see:

http://www.textcheck.com/certificate/nAPsvW

Graphical abstract